Princeton Plasma Physics Laboratory

PPPL-5281

Syntheic Diagnostics Platform for Fusion Plasmas

Lei Shi

June 2016

Prepared for the U.S.Department of Energy under Contract DE-AC02-09CH11466.

Synthetic Diagnostics Platform for Fusion Plasmas[a)]

L. Shi,[1, b)] E. J. Valeo,[1] B. J. Tobias,[1] G. J. Kramer,[1] L. Hausammann,[1] W. M. Tang,[1] and M. Chen[2]
[1)] *Princeton Plasma Physics Laboratory, Princeton, NJ 08540, USA*
[2)] *University of California, Davis*

(Dated: 29 July 2016)

A Synthetic Diagnostics Platform (SDP) for fusion plasmas has been developed which provides state of the art synthetic reflectometry, Beam Emission Spectroscopy, and Electron Cyclotron Emission (ECE) diagnostics. Interfaces to the plasma simulation codes GTC, XGC-1, GTS, and M3D-C[1] are provided, enabling detailed validation of these codes. In this paper, we give an overview of SDP's capabilities, and introduce the synthetic diagnostic modules. A recently developed synthetic ECE Imaging module which self-consistently includes refraction, diffraction, emission and absorption effects is discussed in detail. Its capabilities are demonstrated on two model plasmas. The importance of synthetic diagnostics in validation is shown by applying the SDP to M3D-C[1] output and comparing it with measurements from an Edge Harmonic Oscillation mode on DIII-D.

PACS numbers: 52.70.Gw, 52.65.-y, 52.55.Fa

I. INTRODUCTION

An important goal of current fusion plasma experiments is to validate theoretical models and numerical simulations, so that the plasma behavior in the next generation fusion machines, e.g. ITER, can be predicted with some level of confidence. Many simulation codes now support realistic geometry, so that they can be quantitatively compared with experiments. However, it is difficult to make these comparisons because the physical quantities available from simulations are very different from the measured ones. In simulations, the data is given in plasma quantities, e.g. density and temperature, while experimentally, a set of diagnostics is used to observe the plasma, which do not immediately measure plasma quantities. For instance, the electron temperature can be derived from measured electron cyclotron emission power.

Traditionally, it is the diagnosticians' job to *interpret* the measured signals and provide knowledge about the underlying plasma quantities. But in most cases, the measurements do not contain full information about the original plasma state, and therefore the exact plasma quantities can not be reconstructed from the measurements.

Synthetic diagnostics provide an alternative approach to make theory-experiment comparisons. While interpreting measurements is difficult or even impossible in many cases, *forward modeling* of the diagnostic process can be carried out with the full plasma information given by simulation or theory. In contrast to the interpretation approach, no *a priori* assumptions about the plasma and diagnosing processes are needed since the plasma is known and the diagnostics are simulated. One limitation comes from the models used to simulate the diagnostics. The validity of these models can be independently examined through either theoretical assessments or numerical studies. The synthetic results can then be compared directly to the measured ones, and provide valuable information about both the simulations and experiments.

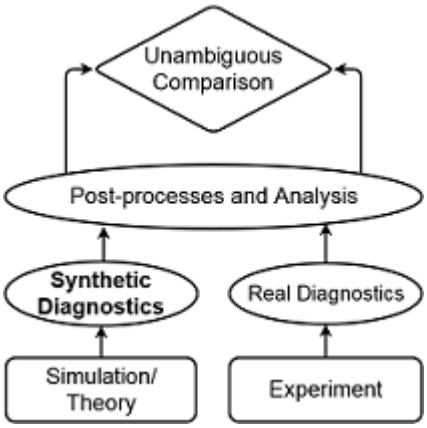

FIG. 1. Synthetic diagnostic work flow.

Figure 1 shows the typical work flow of a complete comparison between simulations and experiments using synthetic diagnostics. Synthetic diagnostics play a central role in this comparison. They transform the output from simulations into the synthetic signals that are then processed in the same way as the measured signals. The synthetic and experimental results can then be compared in an unambiguous way.

Another important usage of synthetic diagnostics is to quantify uncertainties and sensitivities of the underlying

[a)] Invited paper published as part of the Proceedings of the 21st Topical Conference on High-Temperature Plasma Diagnostics, Madison, Wisconsin, June, 2016.

[b)] Electronic mail: lshi@pppl.gov

measurements. They are thus important tools for validation, and fit in the proposed guidelines for best validation practices[1]. In addition, once the diagnostic response is known, the synthetic diagnostics can also be used to optimize diagnostic hardware.[2].

In this paper, we describe the Synthetic Diagnostics Platform (SDP), a platform for both development and application of synthetic diagnostic codes. Its modular structure makes adding new diagnostics straightforward. Programmed in Python, it can benefit from the strong support provided by the Python scientific computing community[3,4]. It is also possible to include C/Fortran code into SDP, enabling further optimizations when high computational efficiency is vital. SDP can read output from various simulation codes, and generate test plasmas based on theoretical models. After the synthetic diagnostic runs, the synthetic signals can be further processed in various analysis and post-process modules. A group of supporting packages provides basic utilities and standard interfaces, including geometry, I/O, and unit conversions.

At present, three synthetic diagnostics are available in SDP: a reflectometry diagnostic based on the FWR codes[5] (Sec. II), a Beam Emission Spectroscopy diagnostic (Sec. III), and an advanced Electron Cyclotron Emission Imaging (ECEI) diagnostic. The ECEI module uses an innovative reciprocal approach[6] to calculate the observed ECE power. It includes refraction, diffraction, absorption and emission effects in one calculation, and is discussed in Sec. IV.

II. SYNTHETIC REFLECTOMETRY

Reflectometry is used to measure electron density profiles and fluctuations[7,8]. It uses the fact that electromagnetic waves with a certain frequency and polarization can propagate in part of the plasma and get reflected back. The relative phase between the reflected wave and a reference wave contains information about the location of reflection, which is in turn related to the local electron density. Millimeter-wave Imaging Reflectometry[9] (MIR) is an extension of traditional reflectometry, which adds lenses and an array of receivers to provide imaging in the radial and vertical direction.

FWR2D is a two dimensional combined WKB/Finite-Difference Time-Domain (FDTD) code solving the electromagnetic wave equation within a two-dimensional plasma, in which a reflection layer exists[5]. It exploits the fact that the probing waves in reflectometry measurement usually propagate nearly perpendicularly to the flux surfaces. Away from the reflection layer, an efficient paraxial/WKB approximation is used to solve for the slow varying amplitude of the wave, while the rapid phase variation is governed by the local dispersion relation. Near the reflection layer, where the WKB approximation breaks down, the time-dependent full wave equation is solved until a steady wave field is established. The code has been verified and validated against experiments[10].

The 3D counterpart FWR3D has a very similar structure as FWR2D , but it allows three dimensional plasma and fields. This enables studies of new physics, such as polarization mixing and magnetic shear effects.

SDP contains interfaces for FWR2D/3D to the GTS[11] and XGC-1[12] simulation codes. Both codes provide plasma data on poloidal planes, and use flux coordinates on each plane. On each toroidal cross-section, SDP uses triangulation and 2D interpolation provided by Scipy[13] to obtain data on a regular Cartesian mesh. Since the fluctuations under study have long parallel wavelengths, we interpolate the data linearly along field line between planes. Post-processing modules are available for converting FWR2D/3D output into a complex amplitude comparable to the signal measured by reflectometers. FWR2D has been widely used as a design and optimization tool for reflectometry systems[14,15].

In a recent study of Edge Harmonic Oscillations (EHOs)[2], a careful comparison between MIR measurements and simulation results of M3D-C^1 code[16] was performed by forward modeling using FWR2D. EHOs are coherent oscillations which are usually observed near the plasma edge in Quiescent H-mode (QH-mode) discharges[17]. They are related to the enhanced transport near the plasma edge, and are believed to be crucial for the suppression of Edge Localized Modes (ELMs).

MIR on DIII-D[9] was used to measure edge electron density perturbation during EHOs. It has 12 vertically separated sightlines, and four frequencies, corresponding to 4 different radial cutoff locations.

The three dimensional resistive MHD simulation code[16] M3D-C^1 was used to study the nature of the EHOs. M3D-C^1 reads in plasma profiles from a DIII-D discharge (shot #157102) and calculates the linear mode structure for a range of toroidal mode numbers. The peak amplitude is set to be 2% of the equilibrium density. Synthetic MIR is then applied to M3D-C^1 data, and a poloidal wave number spectrum is generated for each probing frequency.

Figure 2 shows the comparison between MIR measurement and synthetic MIR result at two frequencies, 57 GHz and 58 GHz, corresponding to two radial locations. Poloidal wave number spectra for the n=1 component of the EHO are calculated based on the phase difference and the vertical distance of each pair of vertical receivers. While a relatively peaked spectrum is measured at 57 GHz, as shown in Fig.2(a), a broad spectrum is observed at 58 GHz, Fig.2(b). This distinctive feature has been successfully reproduced by the synthetic MIR applied to the M3D-C^1 simulation. The location and height of the peak of the spectrum at 57 GHz given by synthetic MIR agrees fairly well with measurement. A more careful comparison requires a quantitative assessment of the uncertainties in the measurement, as well as in the simulation. The latter again relies on the synthetic diagnostic tools. Nonetheless, the comparison shown here

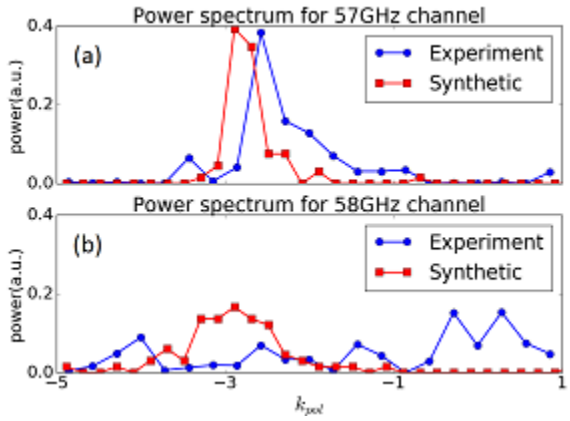

FIG. 2. Measured and synthetic MIR power spectra in poloidal wave numbers with frequencies (a) 57 GHz and (b) 58 GHz for a n=1 EHO in DIII-D shot #157102, at 2420ms.

has demonstrated the potential of synthetic MIR in validation.

III. SYNTHETIC BEAM EMISSION SPECTROSCOPY

Beam Emission Spectroscopy (BES) is a diagnostic method to measure local electron densities. Line emissions resulting from the interaction between the plasma and the injected neutral beam is measured. The intensity of the observed light is proportional to the local electron density in the plasma.[18] A complicating factor in the interpretation of BES signals comes from the fact that excitation and relaxation doesn't happen instantaneously. An excited neutral travels a finite distance before emitting a photon. The size and alignment of receiving optic fibers and lenses can also affect the received intensity. The synthetic BES module on SDP calculates the emission intensity with these effects included and in realistic geometries[19].

The neutral beam density n_b is calculated along the central line of beam using an effective stopping coefficient, S_{cr}, given by Atomic Data and Analysis Structure (ADAS) database[20–22]:

$$v_b \frac{\mathrm{d}n_b(z)}{\mathrm{d}z} = -S_{cr}(z) n_e(z) n_b(z), \tag{1}$$

where n_e is the electron density in plasma, v_b the speed of beam particles, and z the distance along central line of beam. The beam profile in the plane perpendicular to the central line is approximated as a fixed Gaussian function.

The density of the excited neutrals, $n_{ex}(\vec{x})$ is then obtained by solving

$$\vec{v}_b \cdot \nabla n_{ex}(\vec{x}) + \frac{n_{ex}}{\tau} = \langle \sigma v \rangle \, n_b(\vec{x}) n_e(\vec{x}), \tag{2}$$

where $\langle \sigma v \rangle$ is the effective emission coefficient of energy level 3 to 2 given by ADAS[21] and τ is the effective lifetime of the excited state[23].

Eq.2 is derived from the steady state continuity equation for the neutral particles with excitation level 3. The first term is the divergence of the flux, given the velocity field of the beam is divergence free. The second term is the sink of the excited particles, and the RHS term is the source. We use the effective emission rate to be the source because it is proportional to the generation rate of the excited particles in a dynamic equilibrium. Currently, a constant τ is used because its dependency on the electron density is weak when $n_e < 10^{13} cm^{-3}$, which is usually the case at the plasma edge. Inclusion of the density dependency of τ is needed for calculations of emission from the high density regions.

The number of photons emitted per unit volume per unit time, is then $\varepsilon(\vec{x}) = n_{ex}(\vec{x})/\tau_{sp}$, where τ_{sp} is the lifetime due to spontaneous relaxations. The observed intensity, I, is obtained by integration over detection volume of the optic fiber:

$$I = \frac{1}{4\pi} \int \mathrm{d}s \frac{\int_{\Sigma(s)} \varepsilon(\vec{r}) \Omega(s, \mathrm{d}\sigma) \mathrm{d}\sigma}{\int_{\Sigma(s)} \Omega(s, \mathrm{d}\sigma) \mathrm{d}\sigma}, \tag{3}$$

where s denotes the distance along the optical fiber central line of sight, $\Sigma(s)$ the optic fiber's view area at s, and Ω the solid angle of $\mathrm{d}\sigma$ with respect to the optic fiber.

In Figure 3, a comparison between XGC-1 simulated edge electron density fluctuations and synthetic BES signals is shown. The non-instantaneous emission model gives rise to an inward shift, broadening, and a reduction of the signal. These effects can significantly change the observed radial and vertical correlations[19], which are generally used to characterize the underlying density fluctuations. The synthetic BES module can predict and quantify the potential disagreement between the simulations and observations, and provide information about the spatial resolution limits of the BES measurements.

IV. SYNTHETIC ELECTRON CYCLOTRON EMISSION IMAGING

Electron Cyclotron Emission Imaging (ECEI) is a 2D imaging measurement for electron temperatures[24]. Magnetized electrons emit electromagnetic waves with frequencies around harmonics of their cyclotron frequencies, Ω_c. When the electron density is sufficiently large, most of the emission gets reabsorbed. So, measured from outside of the plasma, the emission spectrum near cyclotron harmonics will be blackbody-like. Since the blackbody spectrum is proportional to the temperature in the long wave-length limit, the observed ECE power is

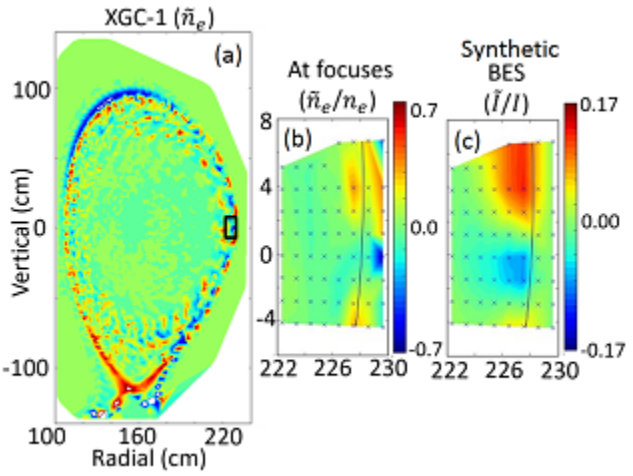

FIG. 3. Comparison between (a) simulated electron density fluctuations, (b) derived n_e fluctuations at the focuses of the BES fibers, and (c) the synthetic BES signal. Note the degradation in spatial resolution and the decrease (different color scale in figs. b and c) in the BES signal.

then closely related to local electron temperature where the emission originates. In magnetically confined fusion devices, the magnetic field strength changes mainly along major radius. So the origin of ECE with frequency ω is localized in the radial direction where $\omega \approx n\Omega_c(R)$. Typically, the harmonic number $n = 2$ is used for ECEI measurements. This feature provides radial resolution for ECE diagnostic. ECEI adds a vertical array of receivers and a set of optical lenses to have vertical resolution, providing a 2D image of the electron temperature[25].

The ECE radiation deviates from the blackbody spectrum near the plasma edge due to the low electron density. This effect gives rise to non-local and density dependent measurements which are observed experimentally[24]. Furthermore, the refraction and diffraction may also become important where the plasma density is high and the emission frequency is close to the local cutoff frequency. The synthetic ECEI2D module addresses these issues by applying a reciprocity theorem for the calculation of the received ECE power[6]. It is an innovative approach that brings the emission, absorption, refraction, and diffraction all together.

The final goal of the code is to calculate the electron cyclotron emission power coming from a given plasma, and collected by a specified external antenna. This problem is difficult to solve because emissions from different plasma locations are incoherent. If we want to solve the diffraction and refraction of the emitted waves self-consistently, we need to solve the wave equation for each individual emission source. For a reasonably resolved 2D mesh, this requires solving the wave propagation equations hundreds of times, which is computationally not feasible. A reciprocity theorem has been introduced to address exactly this problem[6].

Figure 4 shows an illustration of reciprocity theorem. The key insight is that while the original problem is hard to solve, a solution to a reciprocal problem is much easier to find. Consider a time-reversed process where a unit power wave is launched from the antenna, sent back into a "transposed plasma", and is absorbed via the electron cyclotron resonance. The "transposed plasma" is the time-reversed counterpart of the original plasma. It is called "transposed" because the dielectric tensor describing it is closely related to the transpose of the original dielectric tensor. The reciprocity theorem states that the time averaged power $P_s(\omega)$ received by the antenna in the original problem can be calculated using the wave's electric field in the reciprocal problem and a local source current correlation tensor which describes the local emission property of the original plasma.

$$P_s(\omega) = \frac{1}{16}\int_{-\infty}^{\infty} \vec{E}^{(+)}(\omega;\vec{r})\hat{K}(\omega;\vec{r},\vec{r}\,')\vec{E}^{(+)*}(\omega;\vec{r}\,')\mathrm{d}\vec{r}\mathrm{d}\vec{r}\,' \,, \tag{4}$$

where $E^{(+)}$ is the electric field solved in reciprocal problem, $\hat{K}$ the source current correlation tensor of the original plasma.

Solving Eq.4 requires calculating the source current correlation tensor and the electric field in the reciprocal problem. Using this approach, we only need to solve the wave propagation once.

For typical fusion plasmas, the electron cyclotron radius is significantly smaller than the perpendicular wave length of the fluctuations. The electron's parallel motion within one cyclotron period is also small compared to the parallel wave length of fluctuations. This scale separation enables us to use a local uniform formulation for both the dielectric and the source current correlation tensors.

The dielectric tensor is calculated using the weakly relativistic formulation for isotropic magnetized plasmas.[26,27]. The source current correlation tensor $\hat{K}(\omega;\vec{r},\vec{r}\,')$ is calculated from currents, $\delta\vec{j}(\vec{r},\omega)$, produced by uncorrelated discrete magnetized electrons. An ensemble average is then taken over the distribution function in phase space. For consistency with the dielectric tensor, the distribution function is also taken as a weakly relativistic isotropic Maxwellian.

$$\hat{K}(\omega;\vec{r},\vec{r}\,')\delta(\omega-\omega') = 4\left\langle \delta\vec{j}(\omega;\vec{r})\delta\vec{j}^{*}(\omega';\vec{r}\,')\right\rangle . \tag{5}$$

The propagation of the wave launched from the antenna is solved using a paraxial approximation in a similar way as used in FWR2D[5], but with a weakly relativistic dielectric tensor which includes electron cyclotron absorption.

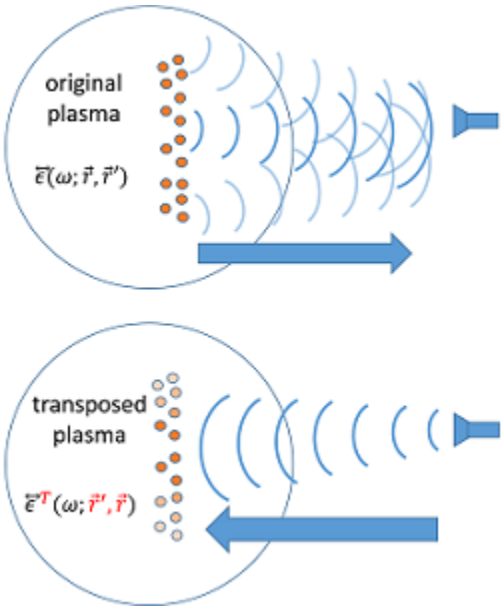

FIG. 4. Illustration of the reciprocity theorem. (a) Original ECE problem. Emissions from many incoherent sources need to be propagated through plasma, and summed up at antenna. (b) Reciprocal problem. A coherent wave is propagated into the "transposed" plasma and is absorbed near the cyclotron resonant layer. The transposed plasma is closely related to the time inverse of the original plasma.

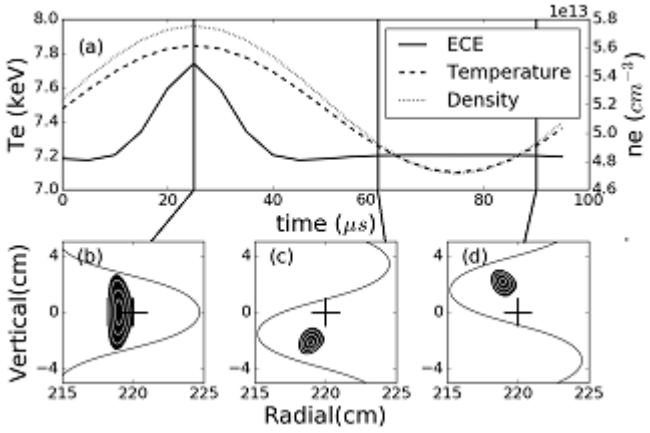

FIG. 5. (a) Synthetic ECE effective temperature(solid), exact electron temperature (dashed) and density (dotted) at the cold resonance as a function of time. Three time snapshots (vertical solid lines) are chosen to show the distinct ECE emission source pattern at different stages. The ECE emission sources (black dot) on top of iso-density contour(black curve) are shown at (b) $20\mu s$, (c) $60\mu s$, and (d) 90 μs. The "+" mark indicates the location of cold resonance in equilibrium.

Both the current correlation tensor and the wave propagation and absorption components of the ECEI2D module have been verified via numerical convergence tests, and benchmarks against theoretical solutions.

With the ability of including the refraction, diffraction, absorption and emission in one calculation, we can now study many non-ideal ECE situations. Two cases are shown below as demonstrations of ECEI2D's capability.

Refraction near cutoff. When the ECE frequency is close to the local cutoff frequency, we expect the refraction effects to be important. We use a simple analytic plasma model to show this effect, in which large electron temperature and density fluctuations ($\tilde{T}_e/T_{e0} = 5\%$, $\tilde{n}_e/n_{e0} = 10\%$) propagate upwards vertically.

Figure 5 shows how the plasma area where the observed emission originates is perturbed by electron density fluctuations. In Fig.5a, a time trace of ECE signal gets squeezed near the peaks of density and temperature fluctuations, and flattened near the troughs. The reason for this can be seen in Figs.5b, 5c, and 5d. From Fig.5c and 5d, we see that the source of ECE tends to stay in the trough of the density perturbation. Since the temperature and density perturbations are in phase, the ECE measured temperature over this period is roughly the same, and leads to the flattened part of the time trace. When the peak of density perturbation is aligned with the unperturbed source location (Fig.5b), the ECE source gets elongated, and moves from the upper trough to the lower trough.

Figure 6 demonstrates the possibility of using ECE measurement for detecting the cross-phase between electron density and temperature fluctuations of a single coherent mode. The strong refraction effect near the cutoff is the key to this application. Fig.6a shows the ECE T_e fluctuation without n_e perturbations. A perfect single frequency mode is seen, indicated by a delta function at the fundamental frequency (10kHz) in the power spectrum, shown in fig 6b. When an in-phase density perturbation is added, as shown in fig 6c, the ECE signal has a flattened trough, and the higher harmonic components show up in the frequency domain, as shown in fig 6d. When the cross-phase ϕ between the density and temperature perturbations is changed to 90°, the flattening region moves to the middle of a period, and a strong second harmonic component is found in the simulation, with almost no fundamental component (Figs. 6e and f). In the $\phi = 180°$ case, the power spectrum looks similar to the $\phi = 0°$ case (Figs. 6g and h).

Shine through effects. When ECE is used to measure H-mode plasma pedestal temperature profiles, the "shine through" phenomena occur[24]. At the bottom of the pedestal, and immediately outside of it, the ECE

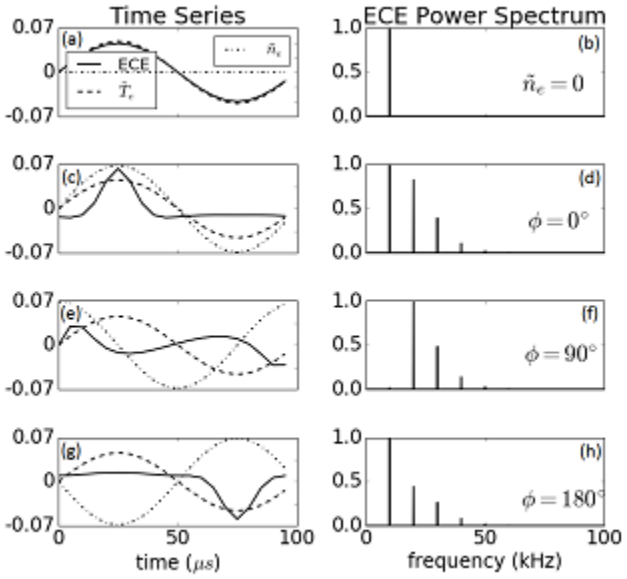

FIG. 6. The time traces and power spectra of synthetic temperature fluctuations under different density-temperature cross phases. The solid lines in plots (a), (c), (e), (g) show synthetic ECE temperature deviations from the time averaged values normalized to the time averaged values. The dashed lines show the electron temperature fluctuations, and the dash-dotted lines show density fluctuations with arbitrary unit. (b), (d), (f), and (h) are the corresponding power spectra of the ECE signals, normalized to the maximum value. (a, b) no density perturbation. 10% density perturbation with (c, d) 0°, (e, f) 90°, and (g, h) 180° cross-phase between $\tilde{n}_e$ and $\tilde{T}_e$.

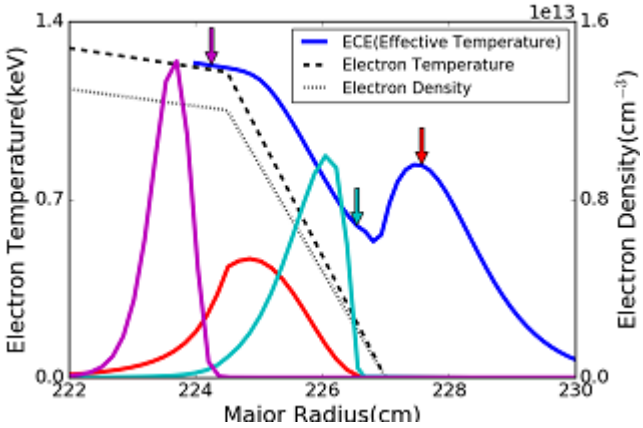

FIG. 7. Synthetic ECE electron temperature profile at the edge of a DIII-D like plasma (solid), the input electron temperature (dashed) and density (dotted). Sources of emission power are shown for optically thick (magenta), gray (cyan) and thin (red) channels. The corresponding cold resonances are indicated with the arrows in the corresponding colors.

observes higher effective electron temperatures than obtained by other diagnostics.

Figure 7 shows a typical shine through case for a DIII-D-like plasma. Three kinds of channels are shown. The optically thick channel, as shown in magenta, is ideal for temperature measurements. The emission comes from a radially localized region right inside the cold resonance. The optically gray channel shown in cyan has a cold resonance at the bottom of the pedestal, and receives the emission power mainly from the lower half of the pedestal. Due to the decrease in optical thickness, this channel receives emission from a source that extends to the mid-pedestal region. The optically thin channel, shown in red, has its cold resonance well outside the pedestal. The emissions from the hotter top pedestal "shine" through the low absorption edge and gets collected by the receiver. As a result, the measured power is even stronger than that from the edge channel (depicted in cyan).

When the density and temperature are perturbed near the edge, the three channels behave differently. The optically thick channel receives mainly blackbody radiation, so it only responds to the temperature fluctuations as expected. The optically gray channel behaves in a complex way. While the local ECE emission power is changing due to the temperature perturbation, the density perturbation affects the optical thickness, and thus controls the non-local depth. An increase in the density will make it optically thicker, and more localized to the pedestal bottom. This tends to lower the measured ECE power. The final result depends on the relative strength and phase of the temperature and density fluctuations. We will see a density dominant example in the next section, where the ECE signal is out of phase with the temperature fluctuations. The shine through channel is also affected by both temperature and density perturbations. However, because it is far from the optically thick regime, an increase in density will always give a larger received power. So it will respond to both temperature and density perturbations positively. We will also see this effect in the next section.

EHO comparison. In this section, we show an application of ECEI2D on the DIII-D EHO case discussed in Sec. II. Figure 8 shows a comparison between the simulated M3D-C^1 results, the synthetic ECEI signals, and the measured ECEI signals. The significant difference between simulation and synthetic results is due to the

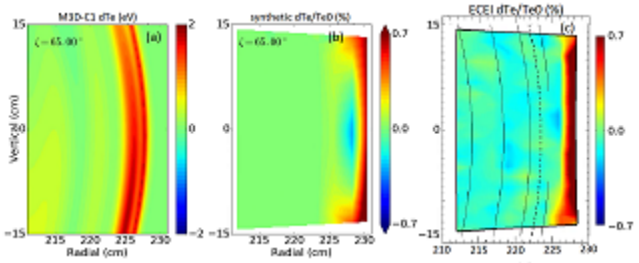

FIG. 8. Comparison between M3D-C[1] simulation (a), synthetic ECEI response (b), and ECEI measurement (c) of electron temperature fluctuations of an EHO (DIII-D, shot #157102 at 2420 ms).

complex response of the ECEI diagnostic in the edge of the plasma. A direct comparison between the simulated δT_e and the measurement interpreted δT_e without using a synthetic diagnostic gives the inaccurate impression that they completely disagree. When the synthetic ECEI diagnostic is applied to the simulated δT_e, the response is in qualitative agreement with the measurements, as shown in Figure 8(b) and 8(c). The strong shine through features are reproduced as well as the out of phase intensity fluctuations at the pedestal bottom.
Although the synthetic and measured signals are in qualitative agreement, they still don't agree quantitatively. The most significant disagreement is the radial location of the shine through layer and the negative response channel. The whole structure of the synthetic signals is shifted about 2cm radially outwards compared to the measured signals. This shift may be due to the uncertainties in the equilibrium reconstruction.

V. SUMMARY

The SDP provides support for both development and application of synthetic diagnostic codes. Synthetic reflectometry, BES, and ECEI modules are currently available on the platform. They have been applied in a number of studies to compare simulations with experiments. Valuable insights about diagnostic techniques were gained by processing results from advanced plasma simulation codes with synthetic diagnostics. A possible way of detecting electron density and temperature fluctuations cross phase has been identified with the new ECEI2D code.

ACKNOWLEDGMENT

This work is supported by the (U.S.) Department of Energy (DOE) under DE-AC02-09CH11466, SC-G903402, DE-FG02-99ER54531, DE-FC02-04ER54698, DE-SC0012551.

[1] P. W. Terry, *et al.* Phys. Plasmas, **15** (2008).
[2] X. Ren, *et al.* J. Inst., **10**, P10036 (2015).
[3] S. v. d. Walt, *et al.* Computing in Science & Engineering, **13**, 22–30 (2011).
[4] F. Prez *et al.* Computing in Science & Engineering, **9**, 21–29 (2007).
[5] E. J. Valeo, *et al.* Plasma Phys. Control. Fusion, **44**, L1 (2002).
[6] A. D. Piliya *et al.* Plasma Phys. Control. Fusion, **44**, 467 (2002).
[7] R. Nazikian *et al.* Rev. Sci. Inst., **66**, 392–398 (1995).
[8] R. Nazikian, *et al.* Phys. Plasmas, **8**, 1840–1855 (2001).
[9] C. M. Muscatello, *et al.* Rev. Sci. Inst., **85** (2014).
[10] G. J. Kramer, *et al.* Review of Scientific Instruments, **74** (2003).
[11] W. X. Wang, *et al.* Phys. Plasmas, **13** (2006).
[12] S. Ku, *et al.* Nucl. Fusion, **49**, 115021 (2009).
[13] E. Jones, *et al.* SciPy: Open source scientific tools for Python (2001–). [Online; accessed 2016-05-17].
[14] G. J. Kramer, *et al.* Nucl. Fusion, **46**, S846 (2006).
[15] X. Ren, *et al.* Rev. Sci. Inst., **85** (2014).
[16] N. M. Ferraro *et al.* J. Comput. Phys., **228**, 7742 – 7770 (2009).
[17] K. H. Burrell, *et al.* Phys. Plasmas, **8**, 2153–2162 (2001).
[18] G. McKee, *et al.* Rev. Sci. Inst., **70**, 2179 (1999).
[19] L. Hausammann. *Development of a Synthetic Diagnostic for Beam Emission Spectroscopy.* Master, Ecole Polytechnique Federale De Lausanne (2015).
[20] H. Anderson. Plasma Phys. Control. Fusion, **42**, 781 (2000).
[21] H. P. Summers. *The ADAS User Manual, version 2.6 http://www.adas.ac.uk* (2004).
[22] K. Ikeda, *et al.* Journal of Plasma and Fusion Research SERIES, **8**, 987–990 (2009).
[23] I. H. Hutchinson. Plasma Phys. Control. Fusion, **44**, 71–82 (2002).
[24] B. J. Tobias, *et al.* Rev. Sci. Inst., **83**, 10E329 (2012).
[25] T. Munsat, *et al.* Appl. Opt., **49**, E20–E30 (2010).
[26] I. P. Shkarofsky. J. Plasma Phys., **35**, 319–331 (1986).
[27] M. Bornatici, *et al.* Nucl. Fusion, **23**, 1153 (1983).

Princeton Plasma Physics Laboratory
Report Disclaimers

Full Legal Disclaimer

Trademark Disclaimer

PPPL Report Availability

Princeton Plasma Physics Laboratory:

http://www.pppl.gov/techreports.cfm

Office of Scientific and Technical Information (OSTI):

http://www.osti.gov/scitech/

Related Links:

U.S. Department of Energy

U.S. Department of Energy Office of Science

U.S. Department of Energy Office of Fusion Energy Sciences

PPPL PRINCETON PLASMA PHYSICS LABORATORY

Princeton Plasma Physics Laboratory
Office of Reports and Publications

Managed by
Princeton University

under contract with the
U.S. Department of Energy
(DE-AC02-09CH11466)

P.O. Box 451, Princeton, NJ 08543
Phone: 609-243-2245
Fax: 609-243-2751

E-mail: publications@pppl.gov

Website: http://www.pppl.gov